

# Magnetization of the joint-free high temperature superconductor (RE)Ba<sub>2</sub>Cu<sub>3</sub>O<sub>x</sub> coil by field cooling

Zheng, Y., Wang, Y., Li, J. & Jin, Z.

Published PDF deposited in Coventry University's Repository

**Original citation:**

Zheng, Y, Wang, Y, Li, J & Jin, Z 2017, 'Magnetization of the joint-free high temperature superconductor (RE)Ba<sub>2</sub>Cu<sub>3</sub>O<sub>x</sub> coil by field cooling', AIP Advances, vol. 7, 095218.

<https://dx.doi.org/10.1063/1.4998230>

DOI 10.1063/1.4998230

ESSN 2158-3226)

Publisher: AIP Publishing

**Open access. All article content, except where otherwise noted, is licensed under a Creative Commons Attribution (CC BY) license (<http://creativecommons.org/licenses/by/4.0/>).**

**Copyright © and Moral Rights are retained by the author(s) and/ or other copyright owners. A copy can be downloaded for personal non-commercial research or study, without prior permission or charge. This item cannot be reproduced or quoted extensively from without first obtaining permission in writing from the copyright holder(s). The content must not be changed in any way or sold commercially in any format or medium without the formal permission of the copyright holders.**

# Magnetization of the joint-free high temperature superconductor (RE)Ba<sub>2</sub>Cu<sub>3</sub>O<sub>x</sub> coil by field cooling

Cite as: AIP Advances 7, 095218 (2017); <https://doi.org/10.1063/1.4998230>

Submitted: 29 July 2017 . Accepted: 11 September 2017 . Published Online: 26 September 2017

Yali Zheng, Yawei Wang , Jianwei Li , and Zhijian Jin

## COLLECTIONS

Paper published as part of the special topic on [Chemical Physics](#), [Energy, Fluids and Plasmas](#), [Materials Science](#) and [Mathematical Physics](#)



View Online



Export Citation



CrossMark

## ARTICLES YOU MAY BE INTERESTED IN

[A finite element model for simulating second generation high temperature superconducting coils/stacks with large number of turns](#)

Journal of Applied Physics **122**, 043903 (2017); <https://doi.org/10.1063/1.4995802>

[Ramping turn-to-turn loss and magnetization loss of a No-Insulation \(RE\)Ba<sub>2</sub>Cu<sub>3</sub>O<sub>x</sub> high temperature superconductor pancake coil](#)

Journal of Applied Physics **121**, 113903 (2017); <https://doi.org/10.1063/1.4978593>

[Non-uniform ramping losses and thermal optimization with turn-to-turn resistivity grading in a \(RE\)Ba<sub>2</sub>Cu<sub>3</sub>O<sub>x</sub> magnet consisting of multiple no-insulation pancake coils](#)

Journal of Applied Physics **122**, 053902 (2017); <https://doi.org/10.1063/1.4997738>

**NEW!**

Sign up for topic alerts

New articles delivered to your inbox





## Magnetization of the joint-free high temperature superconductor (RE)Ba<sub>2</sub>Cu<sub>3</sub>O<sub>x</sub> coil by field cooling

Yali Zheng,<sup>1,2</sup> Yawei Wang,<sup>2,3,a</sup> Jianwei Li,<sup>4</sup> and Zhijian Jin<sup>2</sup>

<sup>1</sup>College of Physical and Electronic Information & Henan Key Laboratory of Electromagnetic Transformation and Detection, Luoyang Normal University, 471934 Luoyang, Henan, China

<sup>2</sup>Department of Electrical Engineering, Shanghai Jiao Tong University, 200240 Shanghai, China

<sup>3</sup>Department of Electronic and Electrical Engineering, University of Bath, BA27AY Bath, UK

<sup>4</sup>Department of Electrical Engineering & Computer Science, University of Liege, 4000 Liege, Belgium

(Received 29 July 2017; accepted 11 September 2017; published online 26 September 2017)

Joint-free (RE)Ba<sub>2</sub>Cu<sub>3</sub>O<sub>x</sub> (REBCO) coil based on ‘wind-and-flip’ technique has been developed to generate a persistent magnetic field without power supply. This paper is to study the magnetization characteristics of the joint-free REBCO coil by field cooling, in order to trap higher field. A joint-free pancake coil is wound by REBCO tapes and the field cooling magnetization test is performed on it. An approximate numerical model based on H-formulation is built for this coil to analyze its magnetization behavior, which is validated by the experimental results. Analysis shows that a persistent direct current is induced in the coil during the field cooling operation, which generates the trapped field. The induced current of the joint-free coil shows an intrinsic non-uniform distribution among turns. Increasing the magnetization field and critical current of REBCO conductors can considerably increase the trapped field. But the trapping factor (the rate of trapped field to background magnetization field) reaches a maximum value (60 % for the test coil). This maximum value is an intrinsic characteristic for a fabricated coil, which only depends on the coil’s geometry structure. With a same usage of REBCO tapes, the trapping factor can be improved significantly by optimizing the coil structure to multiple pancakes, and it can approach 100 %. © 2017 Author(s). All article content, except where otherwise noted, is licensed under a Creative Commons Attribution (CC BY) license (<http://creativecommons.org/licenses/by/4.0/>). <https://doi.org/10.1063/1.4998230>

### I. INTRODUCTION

Second-generation high temperature superconductor (2G HTS) REBCO has always suffered the problem of superconducting joints, which leads to the technique challenges for persistent current REBCO coils.<sup>1-3</sup> The persistent current coil can load a persistent direct current without power supply.<sup>4</sup> The superconducting joint technique has been solved successfully in NbTi and MgB<sub>2</sub> superconductors, but suffers challenges in REBCO conductors because of its complicated molecular structure and processing techniques.<sup>5,6</sup> Although significant progress on REBCO joints has been achieved in 2014, the fabrication method is not easy to be used in industry magnets because of the melted bulk methods used is complicated and time consuming (several hundred hours).<sup>7</sup> A novel coil technique, so-called ‘wind-and-flip’, was proposed to wind a joint-free REBCO coil, which can serve as a persistent current model.<sup>8,9</sup> As shown in Fig. 1, the key idea of this technique is to split a single REBCO tape right down the middle into two tapes, leaving the two ends intact; then the two split tapes serve as the left half and right half of a coil circle respectively.<sup>8,9</sup> This coil enables the current to flow in an absolute superconducting closed loop without any joints. (It can generate a persistent magnetic

<sup>a</sup>Correspondence Author, Electronic mail: [wangyaweisc@gmail.com](mailto:wangyaweisc@gmail.com)

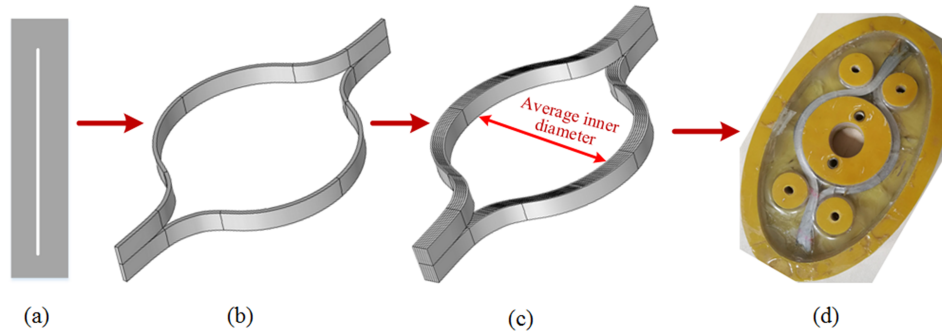


FIG. 1. Schematic illustration of the joint-free REBCO coil from 'wind-and-flip' winding technique. (a) REBCO tape, (b) joint-free single turn, (c) a pancake joint-free coil with multiple turns, (d) photo of the test joint-free coil.

field and works as a HTS magnet, which makes it promising in many HTS applications, such as MRI/NMR, machines, high field magnet and DC induction heaters.<sup>9–21</sup>

Magnetization is the most important issue for this persistent current coil. Field cooling method has been widely used on HTS bulk and stack to trap field.<sup>22–25</sup> It has also been applied on this coil to trap a magnetic field: firstly, the joint-free coil is exposed in a background magnetic field when the coil is above the critical temperature; second, the coil is cooled to superconducting state; then, the background field drops to zero; finally, a stable field is trapped at coil center.<sup>8,9,23</sup> Existing researches focus on the measurement of the trapped field in the field cooling test. Several joint-free HTS coils have been fabricated using REBCO tapes, and the field cooling test was performed. High stable fields are trapped in these tests.<sup>8,26–30</sup> Researches have also focused on the field shielding function of this joint-free coil, which has been validated by experiments.<sup>13,14</sup> Both the field trapping and field shielding result from induced current, and they share a same underlying mechanism.

Existing researches on this joint-free REBCO coil focus on experimental validation of magnetization methods. This paper presents a detailed study on the factors affecting the magnetization of this joint-free coil during field cooling operations, in order to obtain a higher trapped field. An approximate numerical model is built for this coil based on H-formulation method. A single pancake (SP) REBCO coil is wound using the joint-free technique, field cooling tests are performed on it to validate the model. The current and field distribution of the joint-free coil are analyzed using this model. The magnetization mechanism of the joint-free REBCO coil during field cooling operations is analyzed quantitatively. The factors affecting the trapped magnetic field are studied in detail: ramping rate and magnitude of background magnetization field, critical current of the REBCO tapes and the locations of the turns. The trapping factor is analyzed, and measures are proposed to increase the trapped field and trapping factor by field cooling.

## II. EXPERIMENTS AND NUMERICAL MODEL

### A. Field cooling test

A test joint-free coil is wound by REBCO tapes, with 46 turns, as shown in Fig. 1(d). The average inner diameter is 5 mm, as shown in Fig. 1(c). The tape has a width of 10 mm and a thickness of 55  $\mu\text{m}$ , with 306 A self-field critical current (at 77 K in liquid nitrogen). The tape is produced by Shanghai Superconductor Technology Co., Ltd (SSTC). It is split by mechanical method and the split width is less than 0.5 mm. In the field cooling test, first, the coil in normal state is exposed in a uniform background DC magnetic field 50 mT, which is generated by an electromagnet; then the coil is immersed into liquid nitrogen for 300 s, so that it can be cooled to superconducting state completely; after that, the background field is ramped down linearly to zero within 60 s. A hall probe is put at the coil center to measure the magnetic field. Fig. 2 shows the variation of the magnetic field at coil center in this process. The results show that a persistent magnetic field 29 mT is trapped at the coil center after the background field drops to zero.<sup>28,29</sup>

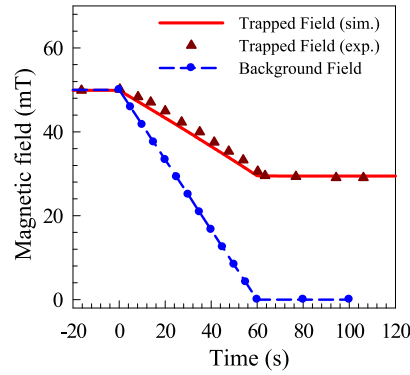


FIG. 2. The magnetic field at the center of the joint-free coil in the field cooling test, from experiments and simulations.

## B. Numerical model

In order to elucidate the electromagnetic behaviors of the magnetization process, a numerical model is built based on finite element method (FEM), as shown in Fig. 3. The ‘eye’-shape turns from ‘wind-and-flip’ winding technique are equivalent to concentric circles with absolute superconducting loop. Therefore, an approximate 2D axisymmetric model is built for the joint-free coil. The model is based on H-formulation of HTS, whose governing equation is as:<sup>31–38</sup>

$$\begin{cases} \nabla \times \mathbf{E} = -\mu \frac{\partial \mathbf{H}}{\partial t} \\ \nabla \times \mathbf{H} = \mathbf{J} \end{cases} \quad (1)$$

$$\mathbf{E} = E_0 \left( \frac{\mathbf{J}}{J_c(\mathbf{B})} \right)^n \frac{\mathbf{J}}{|\mathbf{J}|} \quad (2)$$

where  $E_0 = 1 \times 10^{-4}$  V/m, and  $n=37$  for the REBCO tape in this study.  $\mathbf{H}$  represents the magnetic field.  $\mathbf{E}$  and  $\mathbf{J}$  are electrical field and current density respectively. They show a nonlinear relationship for REBCO conductors, which is represented in Eq. 2.  $J_c$  is the critical current density, whose field dependence is expressed as:<sup>39</sup>

$$J_c(\mathbf{B}) = \frac{J_{c0}}{[1 + \sqrt{(kB_{par})^2 + B_{per}^2/B_c}]^b} \quad (3)$$

where  $J_{c0}$  is the critical current density of the REBCO tape in self-field,  $B_{par}$  and  $B_{per}$  are the magnetic field parallel and perpendicular to the tape surface respectively.  $k$ ,  $b$ ,  $B_c$  are the shape parameters, which is obtained by fitting experimental data. For the REBCO tape in this test,  $k=0.05869$ ,  $b=0.7636$ ,  $B_c=101.7$  mT.<sup>40</sup> Only half-section of the coil is solved in this model due to the symmetry along axial direction. The model is solved by a commercial FEM software Comsol Multiphysics<sup>TM</sup>.<sup>31,35</sup>

The magnetization process in the above field cooling test is simulated by this model, the results is shown in Fig. 2. The magnetic field at coil center drops linearly when the background field decreases

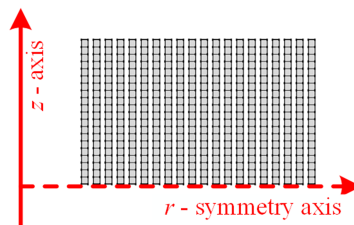


FIG. 3. Schematic illustration of the FEM model for joint-free REBCO coil.

linearly. But the decreasing rate of the field at coil center is lower than that of the background field, and a persistent field is trapped after the background field drops to zero. The results from simulation show a good agreement with that from experiments, which validates the reliability of this model.

### III. MAGNETIZATION MECHANISM BY FIELD COOLING

#### A. Trapping field and induced current

Fig. 4 shows the normalized current density ( $J/J_c$ ) and magnetic field in the REBCO joint-free coil during the field cooling process. Fig. 5 shows the induced current in each turns of the coil and total current induced in all the turns. When the background field begins to drop, an induced current is generated to prevent the reduction of flux linkage. The total induced current increases almost linearly when the background field decreases linearly ( $t < 60$  s), as shown in Fig. 5. A direct current with a total ampere-turn of 1260 A is induced in the coil after the background field drops to zero ( $t > 60$  s). Since circuit loop of the joint-free coil is in superconducting state, the direct current can flow persistently in the coil without any resistance. Therefore, a persistent field is induced by this coil, which is exactly the ‘trapped magnetic field’ measured in experiments.

The persistent current shows an extremely non-uniform distribution among turns, as shown in Fig. 4(a) and Fig. 5. Here, all the turns are numbered 1~46 from the inner turns to the outer turns

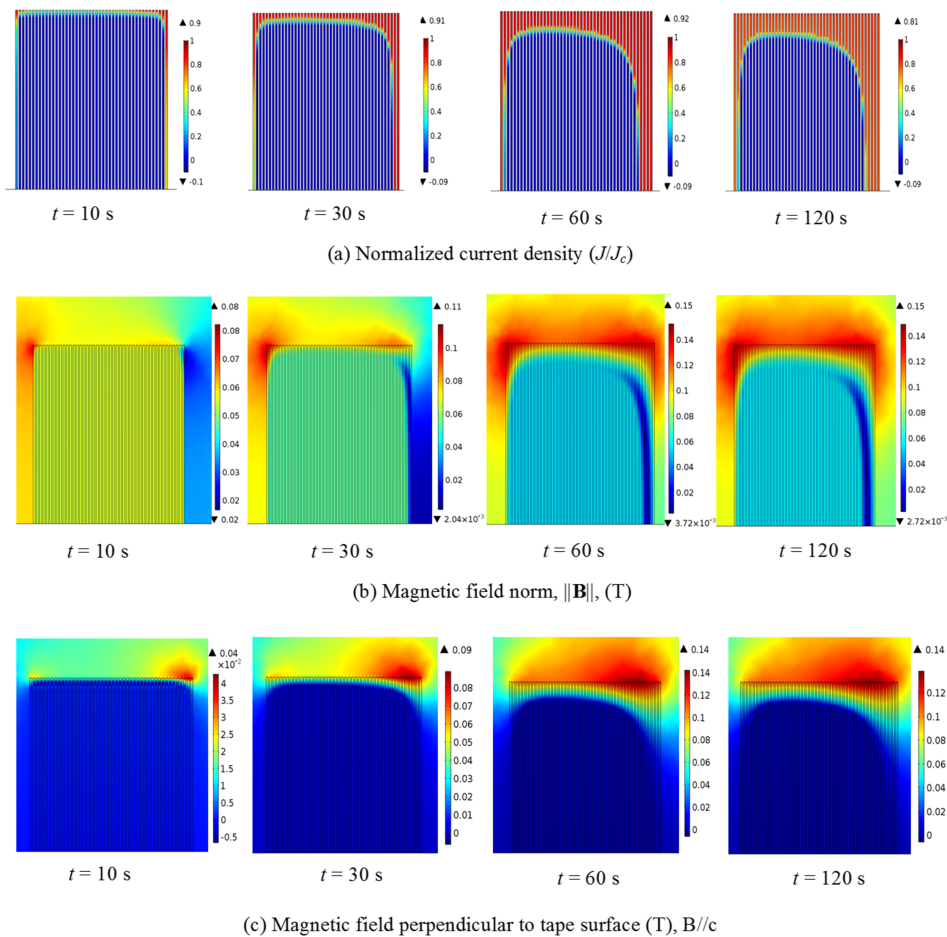


FIG. 4. The distribution of the normalized current density and magnetic field and in the joint-free REBCO coil (*upper half section*).

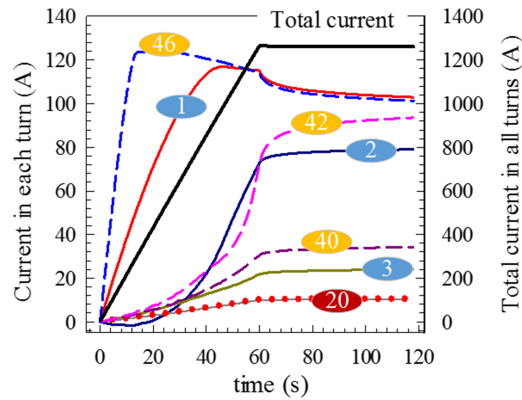


FIG. 5. The induced current in each turn and total induced current in the coil during the field cooling operation, from simulation.

of the coil. When the background field drops, current is induced in turns near the inner and outer side of the coil (1<sup>st</sup> and 46<sup>th</sup> turn) firstly, then neighboring turns follow up. Meanwhile, magnetic field perpendicular to the tape surface ( $\mathbf{B} // \mathbf{c}$ ,  $\mathbf{c}$  is the normal line of the tape surface) is generated on the 1<sup>st</sup> and 46<sup>th</sup> turn firstly, as shown in Fig. 4(c), these turns have a lowest critical current because of the anisotropy of REBCO conductor's critical current. The induced current on the 1<sup>st</sup> turn and 46<sup>th</sup> turn increases rapidly to its critical value ( $J_c$ ) at the early stage of the test ( $t < 10$  s), as shown in Fig. 5. Few currents are induced in other turns in this stage, as shown in Fig. 4(a). The resistance of REBCO conductors increases dramatically to a high value when the induced current approaches to the critical current, which forces the new induced current to generate in other turns with no/lower induced current. Therefore, neighboring turns (45<sup>th</sup> ~42<sup>th</sup> turns and 2<sup>nd</sup> turn) begin to generate induced current. With the increase of total induced current, the magnetic field on the coil increases, as shown in Fig. 4, which leads to the reduction of the critical current of the outer turns (1<sup>st</sup> and 46<sup>th</sup> turns). Therefore, the induced currents on these turns drop slightly in the following process ( $t > 10$  s), as shown in Fig. 5. Meanwhile, the induced currents in middle turns (2<sup>th</sup>~42<sup>th</sup> turn) increase continually. By the end of the field cooling operation, the turns near the inner and outer side of the coil (1<sup>st</sup> and 46<sup>th</sup> turns) induce much higher current than the middle turns.

The resistance of type-I superconductors is nearly zero, which enables a persistent current for years without any measurable degradation. The REBCO conductor is a type-II superconductor, the flux creep and flux flow can result in a very small resistance in REBCO conductors even in superconducting state. This resistance increases with the transport current, which is represented in E-J power law of HTS, as shown in Eq. (2). The resistances of inner and outer turns (1<sup>st</sup> and 46<sup>th</sup> turns) increase with the induced current on them. They increase dramatically to a high value when the induced current approaches to the critical current, which forces the new induced current to generate in other turns with no/lower induced current. Therefore, the obvious non-uniform distribution of the induced current among turns is induced by the turns' location and E-J power law of REBCO conductors.

## B. Degradation of the trapped magnetic field

The resistance of type-I superconductors is nearly zero, which enables a persistent current for years without any measurable degradation. The REBCO conductor is a type-II superconductor, the flux creep and flux flow can result in a very small resistance in REBCO conductors even in superconducting state. This resistance can result in a measureable degradation of the induced current and therefore the trapped field.<sup>30</sup> Fig. 6 shows the decay of the trapped field after the background field drops to zero, in which the ramping time of the magnetization field varies from 1 s to 60 s. Here, the 'magnetization field' is the background magnetic field in which the coil is exposed at the beginning of the field cooling operation. The results show that the trapped field s decays after the field cooling

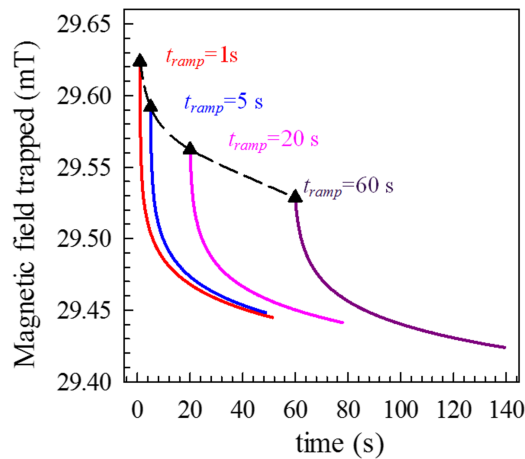


FIG. 6. The decay of the magnetic field trapped at coil center after the field cooling test, magnetization field 50 mT.

test. However, this superconducting resistance is so small that the field decay is very slow and the decay rate drops rapidly with time. In a relatively short term, the joint-free REBCO coil seems to trap a persistent magnetic field. In the above experiments and simulations, there are no apparent changes in the current and magnetic field distribution of the joint-free coil, after the background field disappears absolutely ( $t > 60$  s), as shown in Fig. 2 and Fig. 4. The results also show that the ramping time of the background field has a negligible influence on the trapped field during the field cooling operation.

#### IV. OPTIMIZATION ON THE TRAPPED FIELD

The trapped field is the most important target for the magnetization operation, in which higher trapped field is always preferred. Therefore, it is necessary to study how to increase the trapped field, which is conducted in this section by analyzing the factors affecting it: magnetization field and REBCO conductor's critical current.

##### A. Influence of magnetization field

Simulations are performed on this joint-free coil under different background magnetization fields ranging from 50 mT to 300 mT. All the background fields drop to zero linearly within 10 s. Fig. 7 shows the trapped magnetic field at coil center. The trapped field increases with the magnetization

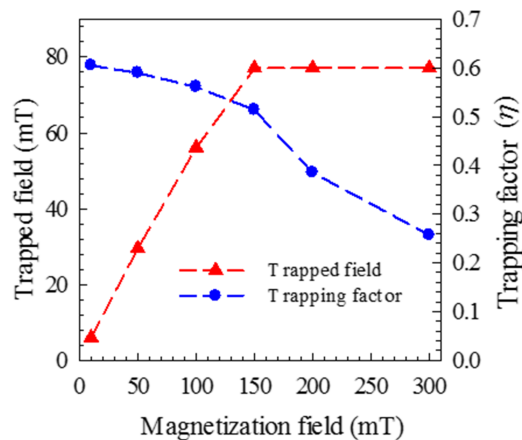


FIG. 7. The dependence of trapped magnetic field at coil center and shielding factor  $\eta$  on the magnetization field.

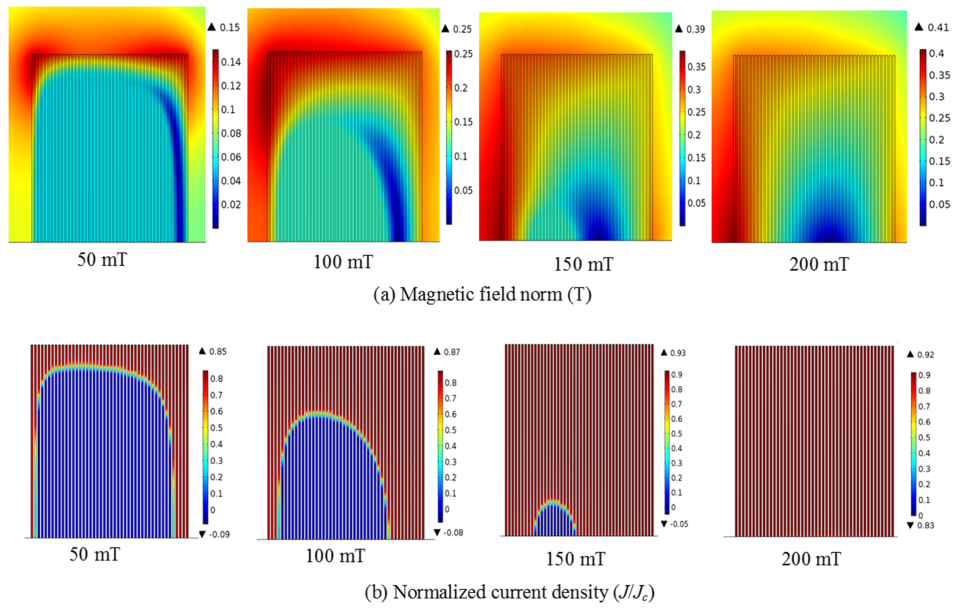


FIG. 8. The magnetic field norm ( $\|\mathbf{B}\|$ ) and normalized current density on the joint-free coil (*upper half section*) after field cooling operation,  $t=20$  s, under different background magnetization field.

field when it is in a low range, which is less than 150 mT for this test coil. Then, the trapped field reaches a maximum value, which is about 77 mT for this test coil. After that, the trapped magnetic field keeps at the maximum value and shows no increase with the further increase of the magnetization field. We define the ‘trapping factor’  $\eta$  as follows:

$$\eta = \frac{B_{trap}}{B_m} \quad (4)$$

where the  $B_{trap}$  is trapped field at coil center after fielding cooling test,  $B_m$  is the magnetization field. The trapping factor drops gradually with the increase of magnetization field though the trapped field increases continually in the same period.

Fig. 8 shows the distribution of the magnetic field norm ( $\|\mathbf{B}\|$ ) and normalized current density ( $J/J_c$ ) on the joint-free coil after the field cooling operation ( $t=20$  s) under different magnetization fields. Fig. 9 shows the induced current distribution among turns at  $t=20$  s. With a low magnetization

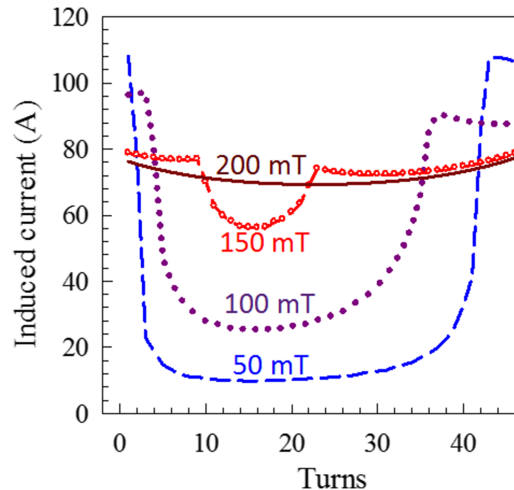


FIG. 9. The induced current among turns after the field cooling test ( $t = 20$  s), under different magnetization fields.

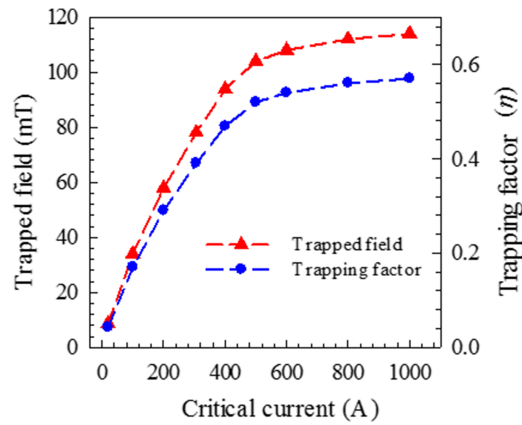


FIG. 10. Dependence of the trapped magnetic field at coil center on the critical current of the REBCO tape, magnetization field 200 mT.

field ( $<100$  mT), there is a significant ‘virgin zone’ without induced current. With the increase of the magnetization field, the virgin zone decreases and more superconducting zones reaches the critical state ( $J/J_c \approx 1$ ) at the end of field cooling operation. When the magnetization field is high enough, which is higher than 150 mT for this test coil, all the superconducting domains reaches the critical state ( $J/J_c \approx 1$ ), and the induced current in each turn increases to the local critical current. The induced current in each turn is limited by the local critical current. The increase of the magnetic field on the joint-free coil results in the decrease of the critical current, and leads to a slight drop on the induced current of the outer and inner turns of the coil (1<sup>st</sup> and 46<sup>th</sup> turn). The maximum value of the coil’s induced current is limited by the critical current of the tape in field. Therefore, the trapped

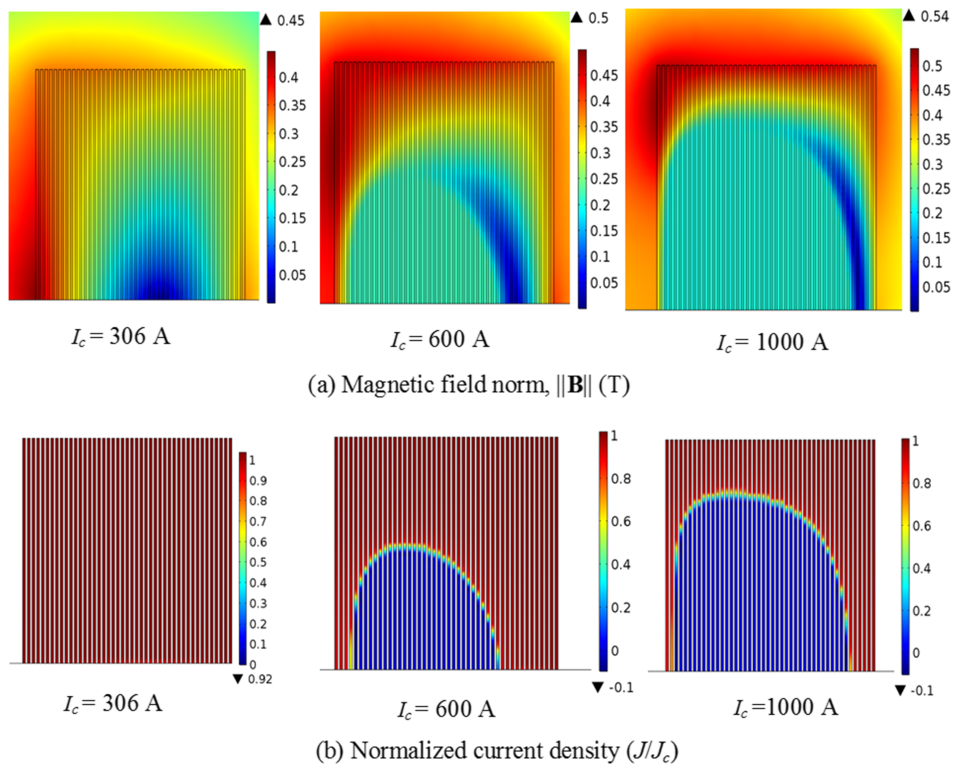


FIG. 11. The magnetic field norm and normalized current density on the joint-free coil (*upper half section*) after field cooling operation,  $t=10$ s, with different critical current, background magnetization field 200 mT.

magnetic field reaches its maximum value, and further higher magnetization field doesn't result in higher trapped field.

## B. Influence of critical current

In above studies, the critical current of the REBCO tape used is 306 A in self-field at 77 K. This section is to study the influence of the tape's critical current on the trapped field. Fig. 10 shows the dependence of the trapped field and trapping factor on the critical current of the REBCO tape used. Here the background magnetization field is 200 mT and it is ramped down to zero within 10 s. The results show that increasing the critical current of the REBCO tape can significantly increase the trapped field when the critical current in a low range ( $I_c < 400$  A for the test coil). Then, the trapped field reaches a saturation value and shows no increases with the further increases of the critical current. The trapping factor shows same trend with the trapped field with the increase of critical current. The maximum trapping factor for this coil is about 60 %.

Fig. 11 shows distribution of the magnetic field magnitude and normalized current on the joint-free coil after field cooling operation,  $t=10$  s. With a low critical current ( $I_c < 400$  A), all the turns of the joint-free coil reach the critical state ( $J/J_c \approx 1$ ) at the end of the field cooling operation, and the induced current is limited by the critical current of the REBCO conductor. The induced current and the trapped field increases with the critical current. Since the local critical current of the REBCO conductor decreases with the external magnetic field, the induced current and the trapped field don't show an absolutely linearly increase with the critical current. When the critical current is high enough ( $I_c > 400$  A), the turns near the inner and outer sides of the joint-free coil show a fielding shielding effect on the middle turns. The superconducting resistances on these turns prevent the further increase of the induced current, therefore, the trapped field reaches a maximum value. The situation is similar to that with a low background magnetization field, as show in Fig. 8.

## V. OPTIMIZATION ON THE TRAPPING FACTOR

The above studies show that the trapped field can be increased significantly by increasing the magnetization field and critical current of the REBCO conductor. However, the trapping factor seems to be limited at about 60 % for the test coil. The maximum trapping factor seems to be an intrinsic characteristic of a fabricated joint-free coil, which cannot be improved by changing the magnetization field and tape's critical current. It happens when the magnetization field is low enough or the conductor's critical current is high enough. In these situations, the trapped field is determined by the induced current, most of which is generated in turns near the inner and outer sides of the coil.

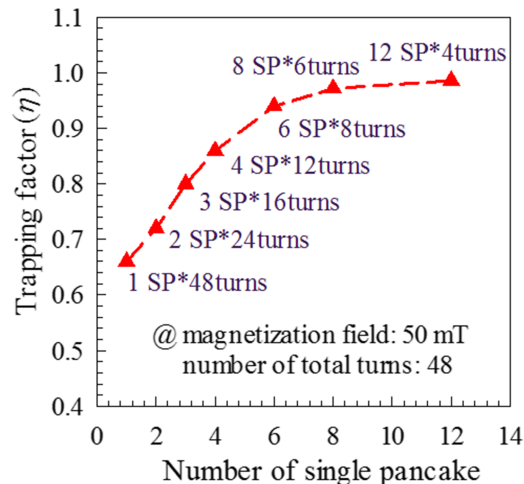
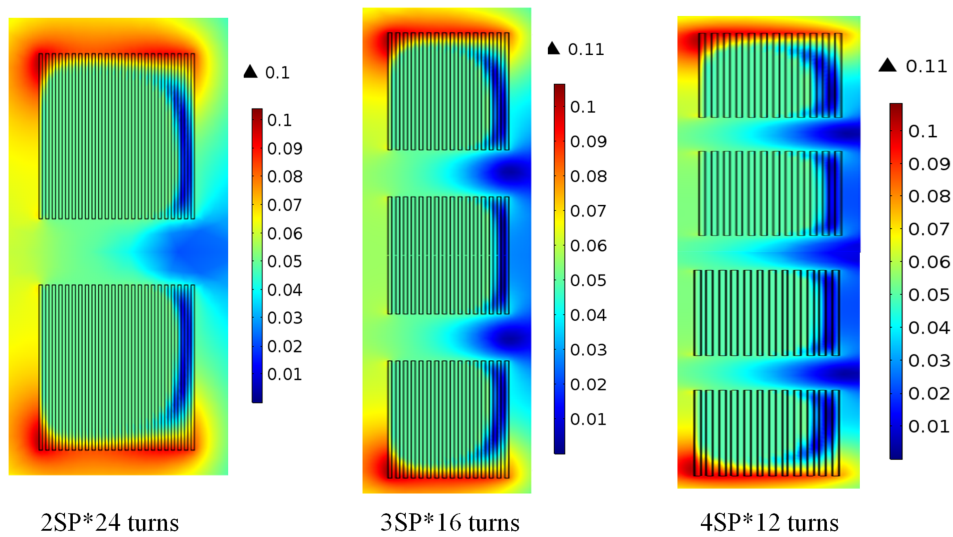


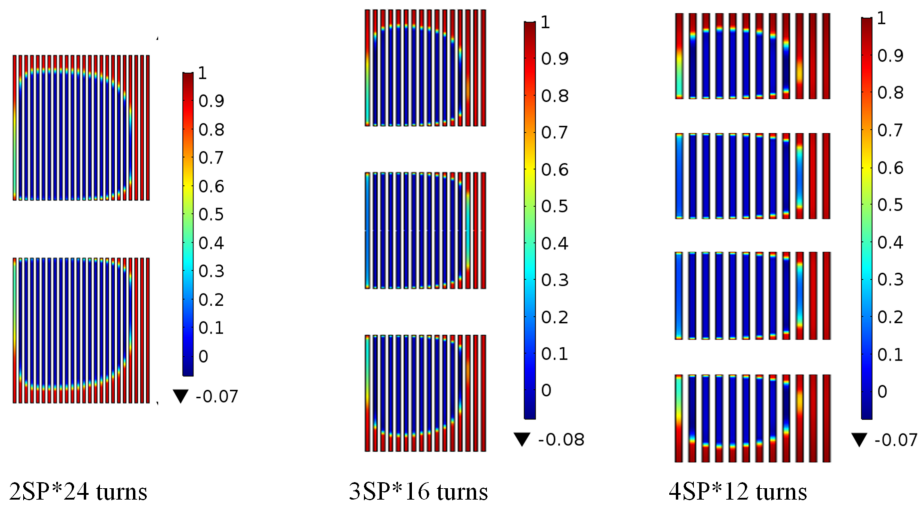
FIG. 12. Dependence of the trapping factor on the number of single pancakes with a same number of total turns.

The current and local critical current of these turns are considerably affected by the locations of the turns. With a same usage of REBCO tapes, the trapping factor may be improved by changing the turns' locations, so that higher magnetic field may be trapped.

The above studies are for a single pancake (SP) joint-free coil with 46 turns. With the same number of total turns, these turns can also be wound to several SP coil with less turns. For a better comparison, 48 joint-free REBCO turns are designed based on the test coil in section II. The REBCO tape here has a thickness of 0.2 mm, which is used more widely in industry applications for a better mechanical performance. All the other parameters are same with that in the test coil. 7 cases are studied: 1×SP coil with 48 turns, 2×SP coil with 24 turns, 3×SP coil with 16 turns, 4×SP coil with 12 turns, 6×SP coil with 8 turns, 8×SP coil with 6 turns and 12×SP coil with 4 turns. All the cases have a same total turns 48. For the multiple joint-free coil system, the distance between adjacent coils



(a) Magnetic field norm,  $\|\mathbf{B}\|$ , (T)



(b) Normalized current density ( $J/J_c$ )

FIG. 13. The magnetic field norm and normalized current density after field cooling operation,  $t=10s$ , number of total turns 48, background magnetization field 50 mT.

is 2 mm. The magnetization field is 50 mT, and it is ramped down to zero linearly within 10 s by the field cooling.

Fig. 12 shows the trapping factor in all cases. Note that, for the multiple SP coil system, the trapped field is that at the center of the axial direction. With a same number of total turns, the trapping factor increases with the number of single pancake coils. It reaches a saturation value when the number of SP coil is large enough. The maximum trapping factor is nearly 100 % for 12×SP coil with 4 turns, which means that the field at the center of the multiple coil system show little decays in the dropping process of the background field. Fig. 13 shows the distribution of magnetic field and normalized current density ( $J/J_c$ ) at the end of the field cooling operation,  $t=10$  s. Here the picture of 3SP×16 turns and 4SP×12 turns is compressed along the axial direction for a better presentation. In the multiple pancake joint-free coil system, the turns near outer side of the coil always generate much more induced current than other turns. The pancakes on the ends have more turns reaching the critical state ( $J/J_c \approx 1$ ) than the middle pancakes.

In a uniform background field, the turns on the outer side of the coil couple more flux linkage than other turns because of larger diameter, and higher voltage is induced on these turns when the background field begins to drop. Current is induced in outer turns first, and field induced by this current compensates the flux reduction of the middle turns, therefore, the induced current in middle turns are prevented. This is the cause of the field fielding effect observed in above studies. The induced current in outer turns is limited by the local critical current, the resistance increases dramatically when the induced current approaches the critical value ( $J/J_c \approx 1$ ). Then the induced current in other turns begins to increase rapidly. With a low magnetization field or high critical current, the induced current on the outer turns accounts for most proportion of the total induced current on the coil, and only these turns reaches critical state ( $J/J_c \approx 1$ ). Therefore, the resistance on the outer turn accounts for most proportion of the total resistances, which determines the total induced current. Since the resistance of the joint-free coil is generated by the non-uniform current distribution, the maximum trapped field is determined by the pancake structure of the joint-free coil, and it cannot be improved by adjusting magnetization field and tape's critical current.

For the designs with more pancakes in Fig. 13, the turns are distributed along the axial direction. The outer turns show less fielding shielding effects on turns of other pancakes, compared to turns of the self-pancake. More turns are exposed at outer sides of the pancakes. In the dropping process of the background field, more current is induced when the current on the outer turns (the 12<sup>th</sup> turn for the 4SP\*12 turns design) reaches to critical value ( $J/J_c \approx 1$ ). With a same total turns, the case with more pancakes generates less resistance. Therefore, the trapping factor increases with the number of pancakes. To increase the trapping factor, the field shielding effect should be minimized by adjusting the locations of turns in the design of a joint-free coil.

## VI. CONCLUSIONS

This paper elucidated quantitatively the physical mechanism for a joint-free coil to trap filed by field cooling. A single pancake joint-free coil was wound by REBCO tapes and field cooling test were performed on it. An approximate numerical model was built to analyze the electromagnetic characteristics of the joint-free coil. It was validated by comparing the trapped fields from simulation and experiments. Factors affecting the trapped field has been studied using this model to trap higher field. Conclusions are achieved as follows:

A persistent current is induced in the joint-free coil when the background magnetization field drops. The induced current shows a significant non-uniform distribution among turns. The turns near the edge side of the coil induce a much higher current than others. The induced current on them reach the critical value ( $J/J_c \approx 1$ ) first, even if the total induced current of the coil is much lower than the critical current of the coil in field. Therefore, they are weakest turns in the magnetization process, which require more attentions in designs.

Second, the ramping rate of the background magnetization field has little influence on the trapped field. The trapped field increases with the magnetization field when it is in a low range. A maximum

trapped field is achieved when the background magnetization field is high enough to make all turns of the coil reach critical state ( $J/J_c \approx 1$ ). Increasing the critical current of the REBCO tape can also increase the trapped field significantly. It reaches a saturation value when the critical current is high enough.

Third, the trapping factor reaches a maximum value when the magnetization is low enough or the tape's critical current is high enough. This maximum value is an intrinsic characteristics for a fabricated coil, and only depends the coil's geometry structure. It can be improved significantly by changing the turns' location. The trapping factor is able to increase to about 100 % by changing a single pancake coil to multiple pancakes. Therefore, the multiple-pancakes structure should be preferred in the industry application of the joint-free REBCO coil. An optimization analysis is required in the design to minimize the tape usage and maximize the trapped field.

- <sup>1</sup> C. A. Baldan, U. R. Oliveira, A. A. Bernardes, V. P. Oliveira, C. Y. Shigue, and E. Ruppert, *Journal of Superconductivity and Novel Magnetism* **26**(5), 2089–2092 (2013).
- <sup>2</sup> J. Lu, K. Han, W. R. Sheppard, Y. L. Viouchkov, K. W. Pickard, and W. D. Markiewicz, *IEEE Transactions on Applied Superconductivity* **21**(3), 3009–3012 (2011).
- <sup>3</sup> Q. Miao, J. M. Zhu, M. Cheng, Z. Zhang, Z. Y. Li, Y. Wang, J. Sheng, Z. Jin, and Z. Hong, *IEEE Transactions on Applied Superconductivity* **25**(3), 1–5 (2015).
- <sup>4</sup> D. Patel, M. S. Al Hossain, K. W. See, W. B. Qiu, H. Kobayashi, Z. Q. Ma, S. J. Kim, J. G. Hong, J. Y. Park, S. Choi, M. Maeda, M. Shahabuddin, M. Rindfleisch, M. Tomsic, S. X. Dou, and J. H. Kim, *Superconductor Science & Technology* **29**(4) (2016).
- <sup>5</sup> D. K. Park, M. C. Ahn, H. M. Kim, H. G. Lee, K. S. Chang, S. J. Lee, S. E. Yang, and T. K. Ko, *IEEE Transactions on Applied Superconductivity* **17**(2), 3266–3269 (2007).
- <sup>6</sup> D. Patel, M. S. Al Hossain, M. Maeda, M. Shahabuddin, E. Yanmaz, S. Pradhan, M. Tomsic, S. Choi, and J. H. Kim, *Superconductor Science & Technology* **29**(9) (2016).
- <sup>7</sup> Y. Park, M. Lee, H. Ann, Y. H. Choi, and H. Lee, *Npg Asia Materials* **6** (2014).
- <sup>8</sup> G. A. Levin, P. N. Barnes, J. Murphy, L. Brunke, J. D. Long, J. Horwath, and Z. Turgut, *Applied Physics Letters* **93**(6) (2008).
- <sup>9</sup> H. G. Lee, J. G. Kim, S. W. Lee, W. S. Kim, S. W. Lee, K. D. Choi, G. W. Hong, and T. K. Ko, *Physica C-Superconductivity and Its Applications* **445**, 1099–1102 (2006).
- <sup>10</sup> J. Kosa, I. Vajda, A. Gyore, and Iop, in *9th European Conference on Applied Superconductivity* (2010), Vol. 234.
- <sup>11</sup> J. Kosa, I. Vajda, A. Gyore, Z. Kohari, and Ieee, *Proceedings of 14th International Power Electronics and Motion Control Conference (Epe-Pemc 2010)* (2010).
- <sup>12</sup> Y. Wang, P. Wang, K. Li, H. Song, J. Yang, C. Ma, Z. Jin, and Z. Hong, *IEEE Transactions on Applied Superconductivity* **27**(4), 3700105 (2017).
- <sup>13</sup> J. F. Fagnard, M. Dirickx, G. A. Levin, P. N. Barnes, B. Vanderheyden, and P. Vanderbemden, *J Appl Phys* **108**(1) (2010).
- <sup>14</sup> L. Wera, J. F. Fagnard, G. A. Levin, B. Vanderheyden, and P. Vanderbemden, *Superconductor Science & Technology* **28**(7) (2015).
- <sup>15</sup> W. S. Kim, Y. Kim, S. H. Park, S. Lee, J. K. Lee, C. Park, B. W. Lee, K. J. Kim, H. Lee, H. G. Lee, G. W. Hong, and K. Choi, *Ieee Transactions on Applied Superconductivity* **20**(3), 1009–1012 (2010).
- <sup>16</sup> J. Kosa and I. Vajda, *Ieee Transactions on Applied Superconductivity* **21**(3), 1388–1392 (2011).
- <sup>17</sup> J. Kosa, I. Vajda, and L. Kovacs, *Ieee Transactions on Applied Superconductivity* **21**(3), 1417–1421 (2011).
- <sup>18</sup> S. Lee, W. S. Kim, Y. Kim, J. Y. Lee, S. H. Park, J. K. Lee, G. W. Hong, S. Kim, J. Han, Y. J. Hwang, and K. Choi, *IEEE Transactions on Applied Superconductivity* **26**(4), 1–4 (2016).
- <sup>19</sup> J. W. Li, M. Zhang, Q. Q. Yang, Z. Y. Zhang, and W. J. Yuan, *Ieee Transactions on Applied Superconductivity* **26**(4) (2016).
- <sup>20</sup> W. S. Kim, S. Lee, Y. Kim, J. Y. Lee, S. H. Park, J. K. Lee, G. W. Hong, J. Han, and K. Choi, *IEEE Transactions on Applied Superconductivity* **25**(3), 1–4 (2015).
- <sup>21</sup> W. S. Kim, C. Park, S. H. Park, J. Lee, J. B. Song, H. Lee, H. G. Lee, G. W. Hong, and K. Choi, *Ieee Transactions on Applied Superconductivity* **19**(3), 2194–2197 (2009).
- <sup>22</sup> S. Kavita and M. Goran, *Superconductor Science and Technology* **26**(11), 115006 (2013).
- <sup>23</sup> Z. Shengnan, M. R. Z. Víctor, A. Baskys, A. Patel, G. Francesco, and B. A. Glowacki, *Superconductor Science and Technology* **30**(1), 014010 (2017).
- <sup>24</sup> S. Zou, V. M. R. Zermeño, and F. Grilli, *IEEE Transactions on Applied Superconductivity* **26**(4), 1–5 (2016).
- <sup>25</sup> A. G. Page, A. Patel, A. Baskys, S. C. Hopkins, V. Kalitka, A. Molodyk, and B. A. Glowacki, *Superconductor Science and Technology* **28**(8), 085009 (2015).
- <sup>26</sup> S. Lee, W. S. Kim, Y. Kim, S. H. Park, J. K. Lee, J. H. Hahn, G. W. Hong, I. H. Park, C. Park, and K. Choi, *IEEE Transactions on Applied Superconductivity* **23**(3), 4601305–4601305 (2013).
- <sup>27</sup> Y. G. Park, C. Y. Lee, J. Lee, S. Nam, Y. D. Chung, Y. S. Yoon, and T. K. Ko, *IEEE Transactions on Applied Superconductivity* **25**(3), 1–4 (2015).
- <sup>28</sup> D. Qiu, W. Wu, Y. Pan, Z. Y. Li, Y. Wang, S. Chen, Y. Zhao, Z. Zhang, P. Yang, X. B. Meng, J. Z. Tian, Y. Q. Zhou, Z. Hong, and Z. Jin, *IEEE Transactions on Applied Superconductivity* **27**(4), 1–5 (2017).
- <sup>29</sup> D. Qiu, W. Wu, Y. Pan, S. Xu, Z. M. Zhang, Z. L. Li, Z. Y. Li, Y. Wang, L. Wang, Y. Zhao, Z. W. Zhang, P. Yang, Z. Hong, and Z. Jin, *IEEE Transactions on Applied Superconductivity* **27**(4), 1–5 (2017).
- <sup>30</sup> C. C. Rong, P. N. Barnes, G. A. Levin, J. D. Miller, D. J. Santosusso, and B. K. Fitzpatrick, *Ieee Transactions on Applied Superconductivity* **25**(3) (2015).

- <sup>31</sup> V. M. R. Zermeno, A. B. Abrahamsen, N. Mijatovic, B. B. Jensen, and M. P. Sorensen, *J Appl Phys* **114**(17) (2013).
- <sup>32</sup> Y. Wang, H. Song, W. Yuan, Z. Jin, and Z. Hong, *J Appl Phys* **121**(11) (2017).
- <sup>33</sup> M. Zhang, J. Kvitkovic, C. H. Kim, S. V. Pamidi, and T. A. Combs, *J Appl Phys* **114**(4) (2013).
- <sup>34</sup> Z. Hong, A. M. Campbell and T. A. Coombs, *Superconductor Science & Technology* **19**(12), 1246–1252 (2006).
- <sup>35</sup> V. M. R. Zermeno and F. Grilli, *Superconductor Science & Technology* **27**(4) (2014).
- <sup>36</sup> F. Grilli and S. P. Ashworth, *Superconductor Science & Technology* **20**(8), 794–799 (2007).
- <sup>37</sup> Y. Wang, M. Zhang, W. Yuan, Z. Hong, Z. Jin, and H. Song, *J Appl Phys* **122**, 053902 (2017).
- <sup>38</sup> V. Lahtinen, E. Pardo, J. Souc, M. Solovyov, and A. Stenvall, *J Appl Phys* **115**(11) (2014).
- <sup>39</sup> F. Grilli, F. Sirois, V. M. R. Zermeno, and M. Vojenciak, *Ieee Transactions on Applied Superconductivity* **24**(6) (2014).
- <sup>40</sup> Y. Wang, C. Wan Kan, and J. Schwartz, *Superconductor Science and Technology* **29**(4), 045007 (045011 pp.) (2016).